The IAGL Land Surface Model

KOEN DE RIDDER AND GUY SCHAYES

Institut d'Astronomie et de Géophysique Georges Lemaître, Université Catholique de Louvain, Louvain-la-Neuve, Belgium

(Manuscript received 4 March 1996, in final form 28 May 1996)

ABSTRACT

A model that computes the fluxes of energy and momentum between the land surface and the atmosphere is presented. It is designed to serve as a lower boundary in a mesoscale atmospheric model and is intended to be used to study the influence of the land surface on regional atmospheric circulations and climate.

The land surface model contains one vegetation layer, a soil skin layer, and four subsurface soil layers. The shortwave and longwave radiation schemes are based on the two-stream theory. Turbulent transfer is treated in a very simple manner, by considering canopy–air and ground–air exchanges separately. Plant water flow is governed by differences in water potential between the soil and the leaves. The stomatal resistance formulation uses the effective leaf area index and the leaf water potential as key variables. It is shown that the resulting transpiration scheme implicitly accounts for the influence of visible radiation, soil moisture, atmospheric saturation deficit, and leaf temperature.

The results of four validation experiments are shown. Parameters were chosen prior to the model runs, and no tuning was involved. These experiments show that the surface model is capable of reproducing observed fluxes within instrumental error including timescales ranging from rapid weather changes up to several months.

1. Introduction

There exists ample evidence of the impact of the land surface on regional atmospheric dynamics and on climate. Among the best known is the albedo–precipitation feedback mechanism forwarded by Charney (1975) to explain the persistence of Sahelian drought. Another feedback mechanism is that based on soil moisture recycling (Walker and Rowntree 1977; Kandel and Courel 1984). Studies by Nicholson (1988) and Lare and Nicholson (1994) confirm the influence of the surface in West Africa in maintaining an anomalously wet or dry situation. Another series of studies (Alpert and Mandel 1986; Otterman et al. 1990; Ben-Gai et al. 1993) suggests a mesoscale climate modification in southern Israel induced by the agricultural development in this region during recent decades. Furthermore, numerical simulations with mesoscale atmospheric models have revealed the importance of differential heating caused by horizontal vegetation and soil moisture gradients in creating regional atmospheric circulations (Yan and Anthes 1988; André et al. 1989; Segal and Aritt 1992).

In section 2 of this paper, a description is given of a land surface model developed at the Institut d'Astronomie et de Géophysique Georges Lemaître (IAGL). The model simulates the physical interactions between the soil, the vegetation, and the atmosphere, and computes how radiation, absorbed by the land surface, is partitioned into other energy fluxes. It is a detailed scheme that properly accounts for the presence of vegetation, designed to replace the existing simple surface parameterizations in the mesoscale atmospheric models MAR (Modèle Atmosphérique Régional) (Gallée and Schayes 1994; Gallée 1995) and TVM (Topographic Vorticity-mode Mesoscale Model) (Schayes et al. 1996; Bornstein et al. 1996), in order to carry out simulations to study the influence of land surfaces on regional atmospheric circulations and climate.

The surface model described here is an updated version of the one described in De Ridder and Schayes (1994). The main improvements took place in the transpiration parameterization. In the new version, plant water flow is based on differences in water potential between the soil and the leaves, as in Federer (1979). Unlike most existing models (e.g., Deardorff 1978; Sellers et al. 1986; Noilhan and Planton 1989; Viterbo and Beljaars 1995) the stomatal resistance formulation does not include empirical functions to account for environmental stresses related to radiation, soil moisture, atmospheric saturation deficit, and leaf temperature. Instead, the stomatal resistance is determined by the ef-

Corresponding author address: Koen De Ridder, Institut d'Astronomie et de Géophysique Georges Lemaître, Université Catholique de Louvain, 2, Chemin du Cyclotron, B-1348 Louvain-la-Neuve, Belgium.
E-mail: deridder@astr.ucl.ac.be
Second author's e-mail: schayes@astr.ucl.ac.be

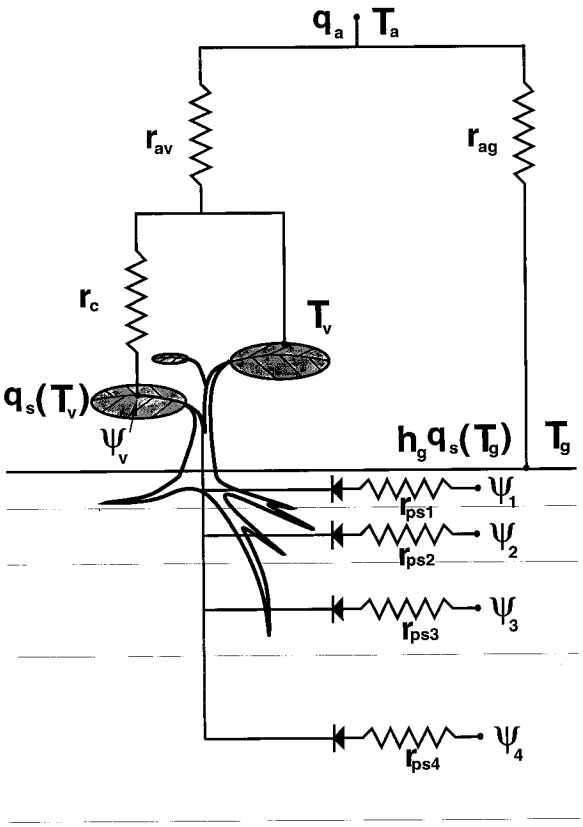

FIG. 1. Schematical representation of the IAGL land surface flux model. The diode symbols represent the fact that water flow is only in one direction: from the roots to the leaves. The combined soil and root resistances are defined as $r_{psi} = (r_p + r_{si})\varphi_i$ where the parameters in the right-hand side of this expression are explained in the text, as are the remaining variables.

fective leaf area index for transpiration and a single empirical function that accounts for the leaf water potential–related stress. It will be demonstrated that this formulation implicitly accounts for the influence of visible radiation, soil moisture, atmospheric saturation deficit, and leaf temperature. The advantage is that reducing the number of empirical functions to a minimum is believed to make the scheme more generally applicable. Furthermore, it will be demonstrated that, in case there is no soil moisture stress, the functional form chosen to account for the leaf water potential–related stress is consistent with Monteith's (1995) conductance model. Another modification with respect to the previous model version is the replacement of the force–restore soil scheme by a five-layer soil scheme for heat and water transport. The turbulent transfer scheme, based on surface-layer similarity theory, as well as the radiation scheme, based on the two-stream equations, have remained essentially unaltered.

In section 3, the results of four validation experiments are shown. It is emphasized that these tests were carried out with parameter sets chosen prior to the model runs and with no tuning involved. They show that the model

TABLE 1. The model parameters to be specified. The following comments refer to the numbers in parentheses. 1) Values of leaf reflectivity and transmissivity are given in Dorman and Sellers (1989). 2) The minimum stomatal resistance r_0 is given a value of 50 s m^{-1} for crops and herbaceous plants, and 100 s m^{-1} for trees and shrubs, in accordance with sources cited in Garrat (1992). 3) For the root fraction in the top 0.1 m of soil we use the following values: $\varphi_{0.1m} = 0.3$ for crops, $\varphi_{0.1m} = 0.5$ for trees and shrubs, and $\varphi_{0.1m} = 0.7$ for herbaceous plants, which is in reasonable agreement with data in Wilson et al. (1987). 4) The plant resistance r_p is given values of $r_p = 5 \times 10^8$ s for crops and herbaceous plants and $r_p = 10^9$ s for trees and shrubs. 5) Soil hydraulic parameters are taken from Clapp and Hornberger (1978).

z_{0m} (m)	Roughness length for momentum
d (m)	Displacement height
L (m^2 m^{-2})	Leaf area index (LAI)
ρ, τ	Leaf reflectivity and transmissivity (1)
g_v	Green leaf fraction
r_0 (s m^{-1})	Minimum stomatal resistance (2)
$\varphi_{0.1m}$	Root fraction upper 0.1 m of soil (3)
r_p (s)	Internal plant resistance (4)
α_{gd}	Dry soil albedo
η_{sat} (m^3 m^{-3})	Soil saturated water content (5)
ψ_{sat} (m)	Soil water potential at saturation (5)
K_{sat} (m s^{-1})	Soil hydraulic conductivity at saturation (5)
b	Soil water retention curve exponent (5)

presented here is sufficiently accurate for use in mesoscale atmospheric modeling studies at timescales ranging from those associated with rapid weather changes up to a month or more.

2. Description of the model

The land surface transfer model, schematically presented in Fig. 1, is one-dimensional (in the vertical) and has one vegetation layer and five soil layers (a soil skin layer and four subsurface soil layers). The energy and water balances are included separately for the soil and the vegetation, as recommended in Camillo (1991). Savijarvi (1992) found that four soil levels combined with the Crank–Nicholson scheme handle well timescales ranging from a few minutes to several days. A fifth layer has been added, in order to encompass the entire root zone and also to include monthly timescales.

When coupled to an atmospheric model, the meteorological input is provided by the wind speed, temperature, and humidity at the first model level, together with the downward shortwave and longwave radiation fluxes, and the precipitation intensity. The returned output consists of the turbulent fluxes of sensible and latent heat, the reflected solar radiation, and the emitted and reflected thermal longwave radiation fluxes, at the land surface. When the model operates off-line, the input is provided by measurements taken in the atmospheric surface layer.

Keeping in mind that the surface model's main purpose is to serve as a subroutine in a mesoscale atmospheric model, the number of parameters to be specified (Table 1) has been kept as small as possible, retaining

only those that were estimated indispensable and that have a reasonable chance of determination at a regional scale, by using soil and vegetation maps and satellite measured reflectances. Besides these variable parameters, the model employs parameters (such as soil emissivity, root diameter, critical leaf water potential, among others) that, because of their limited availability at regional scales, were fixed.

The following sections subsequently describe how the model treats radiative transfer, the turbulent fluxes, transpiration, the surface energy and water balance equations, and the prognostic variables. The subscripts *v* and *g* will be used to refer to the vegetation and ground surface, respectively. By convention, all fluxes are considered positive when directed away from the surface, with an exception made for the radiation fluxes, which are taken positive when directed toward the surface.

a. Radiation transfer

As the incident radiation is the major source for the surface energy fluxes, it is important to know how much of it is absorbed by the soil–vegetation system and how the absorbed energy is shared between both components. The IAGL land surface model uses a radiation subscheme that is based on analytical profiles of shortwave and longwave radiation fluxes in a plant canopy. Its main role is to calculate the shortwave energy fluxes absorbed by the vegetation (R_{sv}) and the ground (R_{sg}) and the net longwave energy flux balance of the vegetation (R_{lv}) and the ground (R_{lg}). (A list of symbols is given in appendix A.) To do so, specification of canopy structural and optical parameters, as well as the amounts of downwelling short- and longwave radiation is required. For a full description of the radiation scheme the reader is referred to De Ridder (1996). The rest of this section gives a summary of that scheme.

The radiation scheme is based on the two-stream approximation, which consists of dividing the diffuse radiation into isotropic upwelling and downwelling components. The main difference with Dickinson's (1983) two-stream model is that, instead of calculating the direct beam upscatter coefficient by adopting the single scattering and semi-infinite canopy approximations, this coefficient is calculated explicitly. Such is more accurate, especially for sparse canopies and for the near-infrared part of the solar spectrum. The required input parameters are the LAI, the green leaf fraction, the leaf optical properties (see comment in Table 1), and a factor describing the leaf angle distribution, which is assumed uniform for simplicity. Another necessary parameter, the ground surface albedo, is parameterized as in McCumber and Pielke (1981):

$$\alpha_g = \begin{cases} \alpha_{gd}\left(1 - \dfrac{\eta_g}{\eta_{\text{sat}}}\right), & \dfrac{\eta_g}{\eta_{\text{sat}}} < \dfrac{1}{2} \\ \dfrac{1}{2}\alpha_{gd}, & \text{otherwise.} \end{cases} \quad (1)$$

Note that in these expressions, it was assumed that the albedo of a totally dry soil surface (α_{gd}) approximately equals twice the albedo of a totally wet soil surface (as apparent from values in Wilson and Henderson-Sellers 1985). A comparison with field data has shown that the error on the radiant energy absorbed by the entire surface is of the order of a few percent, whereas the error on the partitioning of the absorbed energy between the vegetation and the soil is estimated to be of the order of 10%.

The radiation scheme, initially developed for shortwave radiation, has been extended to longwave radiation by including a leaf temperature–dependent source term for the longwave energy emitted by the leaves. The leaf emissivity is fixed at $\epsilon_l = 0.95$, which is shown to yield a canopy emissivity $\epsilon_c \simeq 0.98$ in the case of a full canopy cover. The emissivity of the ground surface is assumed constant: $\epsilon_g = 0.94$, which is an average of values from several sources (see Pielke 1984; Garrat 1992; Monteith and Unsworth 1990).

Probably the most particular feature of the radiation scheme is the computation of an effective leaf-area index L_e, defined as the LAI associated with those leaves that receive sufficient radiation in the 0.4–0.7-μm wavelength band in order for their stomata to open. Indeed, measurements by Shawcroft and Lemon (1973) show that there exists an abrupt transition in leaf stomatal resistance at radiation flux levels close to 20 W m^{-2} in the spectral band 0.4–0.7 μm. Below this critical level, stomatal closure occurs, causing the leaf stomatal resistance to increase to the much higher cuticle resistance. The variable L_e is determined as the sum of 1) the LAI of the level down in the canopy above which the diffuse radiation flux in the 0.4–0.7-μm band is superior to the critical level of 20 W m^{-2}, and 2) the LAI of the leaf surfaces lower down in the canopy that are in the direct solar beam, when the latter exceeds the critical radiation flux level. Generally, under clear sky conditions and for a dense canopy, the calculated L_e reaches a maximum at noon with values slightly above $L_e \simeq 2$. Note that the effective LAI includes both radiation stress effects as well as a radiative shielding factor and does not require empirical functions.

b. The turbulent fluxes

The model contains two heat and moisture sources: the vegetation and the soil surface. It is assumed that both are ventilated separately by surface-layer turbulence, and direct exchanges between the ground surface and the canopy are neglected. This is justified by the fact that the turbulence inside and under the canopy is largely determined by the airflow above the canopy and much less so by the flow in the canopy itself. Indeed, observations suggest that most turbulent transport between the atmosphere and the canopy–ground system occurs in short bursts during which air intrudes from above the plants down into the canopy, and air from

below the canopy is expelled upward (Garrat 1992 and references therein). It appears that most heat and moisture transfer occurs in eddies that have a size that is at least comparable to the vegetation height itself. Therefore, it is not realistic to relate the canopy fluxes to the local gradients that occur inside the vegetation. Other evidence of the invalidity of the local gradient closure approach is the existence of countergradient fluxes inside the vegetation canopy (Denmead and Bradley 1985; Stull 1992).

From surface-layer turbulence theory, the aerodynamic resistances for momentum and heat between the surface and a reference level z_a in the surface layer can be written, respectively, as follows:

$$r_{am} = \frac{1}{k^2 u_a}\left[\ln\left(\frac{z_a - d}{z_{0m}}\right)\right]^2 \mathcal{F}_m^{-1}(\mathrm{Ri}_B) \tag{2}$$

$$r_{ah} = \frac{1}{k^2 u_a}\ln\left(\frac{z_a - d}{z_{0m}}\right)\ln\left(\frac{z_a - d}{z_{0h}}\right)\mathcal{F}_h^{-1}(\mathrm{Ri}_B), \tag{3}$$

where $k = 0.4$ is von Kármán's constant, u_a is the wind speed at the reference level, and $\mathcal{F}_m$ and $\mathcal{F}_h$ are stability corrections (Louis 1979), modified in order to account for $z_{0h} = z_{0v} = z_{0m}/7.4$ (Garrat 1992), which are the roughness lengths for heat, water vapor, and momentum, respectively. Both stability functions depend on the bulk Richardson number Ri_B:

$$\mathrm{Ri}_B = \frac{g(z_a - d)(T_a - T_{\mathrm{eff}})}{T_a u_a^2}, \tag{4}$$

with g the gravitational acceleration. The effective aerodynamic surface temperature T_{eff} is a weighted average of soil and canopy temperatures as will be shown below. The wind stress is defined as

$$\tau = \rho_a u_*^2 = \rho_a \frac{u_a}{r_{am}}, \tag{5}$$

where ρ_a is the air density and u_* the friction velocity.

Since little is known about canopy turbulence, it is simply assumed that the ventilation of the canopy is proportional to its fractional cover. The latter is defined as the vertical projection of the canopy elements onto a horizontal plane and, for uniformly distributed leaf positions and leaf angles, is given by

$$\sigma_v = 1 - e^{-L/2}, \tag{6}$$

where the symbol L stands for the LAI.

As the model treats the turbulent transfer from the canopy and the ground surface separately, the aerodynamic resistances corresponding to either source are parallel. This way, the vegetation and ground aerodynamic resistances for heat can be written, respectively, as

$$r_{av} = \frac{r_{ah}}{\sigma_v} \tag{7}$$

$$r_{ag} = \frac{r_{ah}}{1 - \sigma_v}. \tag{8}$$

Now, the total sensible heat flux can be written as

$$H_a = H_v + H_g \tag{9}$$

$$= \rho_a c_p \frac{T_v - T_a}{r_{av}} + \rho_a c_p \frac{T_g - T_a}{r_{ag}}, \tag{10}$$

where T_v and T_g are the canopy and ground temperature, respectively, and c_p is the specific heat of air at constant pressure. The surface sensible heat flux can also be written as

$$H_a = \rho_a c_p \frac{T_{\mathrm{eff}} - T_a}{r_{ah}}, \tag{11}$$

thus implying

$$T_{\mathrm{eff}} = \sigma_v T_v + (1 - \sigma_v) T_g. \tag{12}$$

Note that T_{eff} can be thought of as an effective aerodynamic turbulence surface temperature, which is, in general, not the same as the radiative surface temperature. This is important when comparing simulated surface temperatures with those obtained from satellite-measured radiances.

The latent heat flux can be decomposed into vegetation and ground contributions as follows:

$$L_v E_a = L_v E_v + L_v E_g \tag{13}$$

$$= L_v(E_{\mathrm{dir}} + E_{\mathrm{tr}}) + \rho_a L_v \frac{h_g q_{\mathrm{sat}}(T_g) - q_a}{r_{ag}}, \tag{14}$$

where L_v is the latent heat of vaporization for water and $q_{\mathrm{sat}}(T_g)$ is the saturation specific humidity at the ground surface temperature. The ground surface relative humidity h_g is defined as a function of ψ_g, the soil water potential (see below) at the ground surface:

$$h_g = \exp\left(\frac{g\psi_g}{R_w T_g}\right), \tag{15}$$

R_w being the gas constant for water vapor. The canopy evaporation flux is subdivided in a direct component and a transpiration component. Indeed, a canopy that is partially wetted by dew or intercepted rain evaporates the intercepted water, resulting in a direct vapor flux, E_{dir}, whereas the dry fraction of the vegetation transpires, giving rise to a transpiration vapor flux E_{tr}:

$$E_{\mathrm{dir}} = \rho_a \delta \frac{q_{\mathrm{sat}}(T_v) - q_a}{r_{\mathrm{av}}} \tag{16}$$

$$E_{\mathrm{tr}} = \rho_a (1 - \delta) \frac{q_{\mathrm{sat}}(T_v) - q_a}{r_{av} + r_c}. \tag{17}$$

The wet fraction is defined as $\delta = w_v/w_{v\mathrm{max}}$, where w_v is the amount of intercepted water, to be discussed further, and $w_{v\mathrm{max}}$ is a threshold value above which throughfall of rain to the ground occurs and is taken equal to 0.2 kg m^{-2} L (Garrat 1992). The stomatal resistance r_c will be treated in the next section.

c. Transpiration parameterization

The key variable used to model the transpiration process is the leaf water potential ψ_v (expressed as a negative height), which is assumed representative for the canopy as a whole. This variable regulates the flow of water from the soil to the canopy and farther on to the atmosphere. It is assumed that the flow of water is in one direction only, that is, from the soil to the leaves (this flow direction is taken as positive). This excludes excretion of water by the roots or intake of water by the stomatal openings. This also means that water can be extracted only from soil layers at a higher (less negative) water potential than the leaves.

The water flow through the plant is written as the sum of the transpiration fluxes from each of the soil layers, as in Federer (1979). These fluxes are proportional to the difference in water potential between the leaves and the corresponding soil layer:

$$W_v = \sum_{i=1}^{4} W_{vi} \tag{18}$$

$$= \sum_{\substack{i=1 \\ \psi_i > \psi_v + d}}^{4} \rho_w \varphi_i \frac{(\psi_v + d) - \psi_i}{r_p + r_{si}}, \tag{19}$$

where ρ_w is the density of liquid water and ψ_i is the soil water potential of the ith layer. Note that the layers are numbered starting at the upper layer with finite thickness, thus excluding the skin surface layer. The parameter r_p was previously defined as the internal plant resistance. The soil–root resistance r_{si} is computed using Cowan's (1965) root model with a root diameter of 0.00035 m and a total root length per unit surface of 4000 m m^{-2}. This is close to values cited by Federer (1979) and Sellers and Dorman (1987), yielding

$$r_{si} = \frac{0.0001 \text{ m}}{K(\eta_i)}, \tag{20}$$

where $K(\eta_i)$ is the hydraulic conductivity calculated as a function of the soil water content η_i of the ith soil layer (see below). The root fraction per layer φ_i is computed from the parameter $\varphi_{0.1\text{m}}$, defined as the fraction of the roots in the upper 0.1 m of soil. To do so, it is assumed that the roots are distributed with depth according to uniform profiles in the layer between the surface and 0.1-m depth and the layer between the 0.1- and 1.0-m depths. This allows interpolation of the root fractions toward the model layers.

The canopy stomatal resistance, which appeared in the definition of E_{tr} (previous section), is computed as follows:

$$r_c = \frac{r_0}{L_e} F_{\text{st}}(\psi_v), \tag{21}$$

where r_0 is the minimum (unstressed) stomatal resistance of a leaf and L_e was previously defined as the leaf area index associated with those leaves that receive enough visible light to maintain their transpiration. The leaf water potential dependence is parameterized as follows:

$$F_{\text{st}}(\psi_v) = \left(1 - \frac{\psi_v}{\psi_c}\right)^{-1}. \tag{22}$$

The parameter ψ_c is the value of the leaf water potential at which total stomatal closure occurs. Following data presented in Federer (1979) and Wetzel and Chang (1988), a value of $\psi_c = -250$ m was adopted.

Note that, although relatively simple, the formulation described in this section implicitly takes into account the dependence of stomatal resistance on visible solar radiation (through L_e), soil water stress, leaf temperature, and humidity saturation deficit (the latter three through the ψ_v-based formulation, as shown in appendix B); all this in a physically consistent and simple manner. Another advantage of this simple ψ_v-based formulation is that when soil moisture is abundant, it is consistent with Monteith's (1995) conductance model (see appendix B).

d. The energy and water balance equations

For both the canopy layer and ground surface layer, energy and water conservation principles must be satisfied. Putting together the energy and water balance equations for the canopy and the ground surface gives rise to a system of four coupled nonlinear equations:

$$R_{sv} + R_{lv}(T_v, T_g) = H_v(T_v, T_g) + L_v E_v(T_v, \psi_v, T_g) + S_v(T_v) \tag{23}$$

$$0 = E_{tr}(T_v, \psi_v, T_g) + W_v(\psi_v) \tag{24}$$

$$R_{sg} + R_{lg}(T_g, T_v) = H_g(T_g, T_v) + L_v E_g(T_g, T_v, \psi_g) + G_g(T_g) \tag{25}$$

$$0 = E_g(T_g, T_v, \psi_g) + W_g(\psi_g). \tag{26}$$

This system is resolved simultaneously for the four unknowns T_v, ψ_v, T_g, and ψ_g with the Newton–Raphson iteration technique for systems of nonlinear equations. We prefer the iterative approach to the use of prognostic equations for the following reasons.

- The iterative approach is more accurate, especially when the forcing variables undergo rapid changes.
- Given the low heat capacity of the vegetation elements, a prognostic equation has to satisfy stringent stability conditions, thus severely limiting the time step.
- The use of prognostic equations for the ground surface would require a finite thickness of the upper soil layer. The iterative approach allows the use of an infinitesimally thin upper soil layer, which is more realistic because of the large temperature and soil moisture

gradients that exist close to the ground surface.

- The iterative approach has a sort of natural time step. Indeed, the number of iterations required to obtain convergence depends on how close the initial guess is to the equilibrium values of the four variables T_v, ψ_v, T_g, and ψ_g, where the initial guess for the first iteration is provided by the values that closed the balance equations at the previous time step. When the forcing variables vary slowly, very few iterations are required. When the forcing changes abruptly, for example, when it starts raining, more iterations are required. Also, when a longer model time step is used, the iteration scheme needs more steps to reach convergence.
- A potential disadvantage of the iterative approach is that convergence is not necessarily assured. However, that is taken care of by employing Davidenko's method (see Ralston and Rabinowitz 1978).

The fluxes G_g and W_g that appear in the soil surface balance are the upper boundary conditions for the prognostic equations for heat and water transfer in the soil, and will be treated in the next section. The heat storage in the canopy is parameterized assuming that the vegetation's heat capacity corresponds to 1 kg m^{-2} of water per unit LAI (Garrat 1992) and also accounts for the water stored on the leaves (w_v, see next section) after rainwater interception:

$$S_v = c_w(w_v + w_l)\frac{\partial T_v}{\partial t}, \tag{27}$$

where c_w is the specific heat of water and $w_l = 1$ kg m^{-2} L. Model simulations show that heat storage is generally small compared to the other canopy energy balance components, almost never exceeding values of a few tens of watts per square meter. The energy associated with photosynthesis is assumed sufficiently small as to justify its neglect in the canopy energy balance equation.

e. The prognostic equations

The canopy water content is determined with a prognostic water balance equation:

$$\frac{dw_v}{dt} = \sigma_v \times \text{rain} - E_{\text{dir}}, \tag{28}$$

where the variable ''rain'' represents the incident rainwater flux. Whenever the canopy's water-holding capacity is exceeded ($w_v > w_{v\max}$, see above), the excess water drips from the leaves to the ground, contributing to a water flux ''drip.'' Note that it is assumed that rain falls vertically, which means that interception of rain by the canopy can be treated the same way as direct light incident at zero zenith angle, which explains the factor σ_v in the last equation.

The equations that describe thermal and hydraulic transport processes in the soil are discretized on four subsurface soil layers with thicknesses d_i ($i = 1,..., 4$). Layer average values are assumed to occur at the layer midlevels. The profiles between midlevels are approximated by linear segments. The computation of the soil moisture–dependent transfer coefficients (thermal and hydraulic conductivity) requires soil moisture values at the layer interfaces. These are obtained by interpolating the piece-wise linear moisture profiles to their interfacial values. To avoid nonlinear equations, the transfer coefficients are computed from soil moisture values obtained at the previous time step. Whenever the soil moisture changes rapidly, as is the case for rain infiltration, a shorter time step is used for the soil heat and water transfer equations such that using the soil moisture from the previous time step is still a reasonable approximation. For the rest of this section, the variable $z_s = -z$ will be employed as vertical coordinate (i.e., pointing downward, and with origin at the soil surface).

Transfer of heat in the soil is calculated by means of the thermal diffusion equation:

$$\frac{\partial T}{\partial t} = \frac{1}{(\rho c)_s}\frac{\partial}{\partial z_s}\left[\mu(\eta)\frac{\partial T}{\partial z_s}\right]. \tag{29}$$

The volumetric heat capacity of the soil is computed as a weighted average of the heat capacities of the soil substrate and the water in the soil, neglecting the specific heat of the air in the pores, as in Pielke (1984):

$$(\rho c)_s = [(1 - \eta_{\text{sat}})1.2 + 4.2\eta] \times 10^6 \text{ J m}^{-3} \text{ K}^{-1}. \tag{30}$$

The soil thermal conductivity is parameterized following Al Nakshabandi and Kohnke (1965) and can, after some algebraic manipulation, be written as

$$\mu(\eta) = 3.81 \text{ W m}^{-1} \text{ K}^{-1}\left[\frac{-\psi(\eta)}{1 \text{ m}}\right]^{-0.4343}, \tag{31}$$

where $\psi(\eta)$ is the soil water potential (see below). The lower limit of the soil thermal conductivity is set to 0.172 W m^{-1} K^{-1}. The soil thermal diffusion equation, discretized on the four layers, is solved with the Crank–Nicholson finite-difference scheme.

The boundary condition at the top of the domain is obtained by specifying the soil surface heat flux:

$$G_g = \mu(\eta_1)\frac{T_g - T_1}{0.5d_1}. \tag{32}$$

At the lower boundary, a zero heat flux is imposed. Notice that the soil thermal conductivity is computed as a function of the water content in the first layer and not as a function of an intermediate moisture value between the first layer midlevel and the ground surface. In most cases, the former will overestimate the thermal conductivity. However, this compensates for the underestimation of the temperature gradient near the soil surface, which results from approximating the moisture profile linearly.

Transport of liquid water in the soil is computed by means of Richard's equation, completed with a transpiration extraction term. Using the soil water content as an independent variable, one obtains a diffusion–gravitation equation, including a transpiration sink term:

$$\frac{\partial \eta}{\partial t} = \frac{\partial}{\partial z_s}\left[D(\eta)\frac{\partial \eta}{\partial z_s} - K(\eta) - \frac{W(z_s)}{\rho_w}\right]. \quad (33)$$

The first term on the right-hand side is a diffusion term, the second represents gravitational flow, and the last is the integrated transpiration water flux between the ground surface and the level z_s. The soil water potential and hydraulic conductivity are expressed as functions of the soil water content following Clapp and Hornberger:

$$\psi(\eta) = \psi_{\text{sat}}\left(\frac{\eta_{\text{sat}}}{\eta}\right)^b \quad (34)$$

$$K(\eta) = K_{\text{sat}}\left(\frac{\eta}{\eta_{\text{sat}}}\right)^{2b+3}. \quad (35)$$

The soil hydraulic diffusivity is computed as (Hillel 1971):

$$D(\eta) = K(\eta)\frac{\partial \psi}{\partial \eta} = -\frac{bK_{\text{sat}}\psi_{\text{sat}}}{\eta_{\text{sat}}^{b+3}}\eta^{b+2}. \quad (36)$$

The finite-difference analog of the water transport equation uses a Crank–Nicholson scheme for the diffusion term and an explicit scheme for the gravitational term. Discretization of the transpiration extraction term introduces the water fluxes W_{vi}, defined in the section describing the transpiration parameterization.

The moisture boundary condition at the top is obtained by specifying the soil surface water flux W_g:

$$W_g = \rho_w D(\eta_1)\frac{\eta_g - \eta_1}{0.5d_1} + \rho_w K_g. \quad (37)$$

When it rains it is assumed that $W_g = (1 - \sigma_v)$ rain + drip, unless this flux exceeds the maximum infiltration rate $W_{g\max}$, defined as

$$W_{g\max} = \rho_w D_{\text{sat}}\frac{\eta_{\text{sat}} - \eta_1}{0.5d_1} + \rho_w K_{\text{sat}}, \quad (38)$$

in which case excess water is discarded as runoff. At the lower boundary, there is the choice between free drainage (zero moisture gradient but gravitational drainage allowed) or impeded flow (no moisture flux at all).

3. Model validation

To validate the land surface model, simulated variables were compared with observations. Relatively long validation periods were chosen (at least from the atmospheric mesoscale timescale point of view) ranging from six days up to four months, for a variety of surface types and meteorological conditions, including rainfall. Long-term validations are believed to be a severe test for model performance, especially for those routines that compute the redistribution of infiltrated rainwater and the subsequent transpiration by the plants. Furthermore, they demonstrate the model's behavior at timescales of a month or so, which will be an advantage when carrying out mesoclimatic simulations in the future.

In all validations described here, a time step of 300 s and layer thicknesses of 0.02, 0.06, 0.20, and 0.72 m for the soil were used. The forcing variables are the incoming shortwave and longwave radiation, the wind speed, temperature and humidity at a level within the surface layer, and the precipitation intensity. In all validations, except HAPEX–MOBILHY (Caumont), the downward thermal infrared radiation flux was not available. This quantity was therefore parameterized following Brutsaert (1982) as a function of the vapor pressure and the temperature at the reference level z_a, including a correction for cloudiness. The cloud fraction was estimated by inverting a relationship expressing the downward solar radiation as a function of the solar zenith angle and the cloud fraction, as in Groot and King (1993). Also, for most validations the initial soil temperature was not available. In that case, the temperatures of the upper and lower soil layers were initialized with the instantaneous and mean values (over the previous 24-h period) of the air temperature, respectively. The temperatures of the layers in between were linearly interpolated between these values. Initialization of soil moisture content will be discussed separately for every validation.

It is emphasized that in all the validations shown hereafter, the parameters (specified in Table 2) were chosen prior to the model runs, and no tuning of model parameters was done. The canopy structural parameters z_{0m}, d, and L were specified case by case, mostly from observations by the teams that did the micrometeorological measurements. The leaf optical properties ρ and τ were taken from Dorman and Sellers (1989). The green leaf fraction was set to unity for all validation cases. The transpiration related parameters r_0, $\varphi_{0.1\text{m}}$, and r_p were given the vegetation type–dependent values as mentioned in Table 1. The dry soil albedo α_{gd} was given a value of 0.30. The soil hydraulic parameters η_{sat}, ψ_{sat}, K_{sat}, and b were taken from Clapp and Hornberger (1978) as a function of soil type in the USDA classification scheme. It is also recalled that the stomatal resistance formulation contains no explicit dependence on leaf temperature or saturation deficit, these effects being implicitly accounted for by the ψ_v-based parameterization, as shown in appendix B.

a. HAPEX–MOBILHY (Caumont) 25–30 June 1986

This validation uses data collected by one of the SAMER stations during the HAPEX–MOBILHY (André et al. 1986) special observation period over a soybean field. The SAMER micrometeorological stations were operated

TABLE 2. Parameters used in the validation experiments. The subscripts ''vis'' and ''nir'' refer to the visible and near-infrared parts of the solar spectrum, respectively.

Parameter	Caumont	Landes	IAGL	ARME
z_{0m} (m)	0.025	1.6	0.01	2
d (m)	0.18	14	0.07	21
L	3.2	6.0	3.5	6.0
ρ_{vis}, ρ_{nir}	0.11, 0.58	0.07, 0.35	0.11, 0.58	0.10, 0.45
τ_{vis}, τ_{nir}	0.07, 0.25	0.05, 0.10	0.07, 0.25	0.05, 0.25
g_v	1.0	1.0	1.0	1.0
r_0 (s m^{-1})	50	100	50	100
$\varphi_{0.1m}$	0.3	0.5	0.7	0.5
r_p (s)	5×10^8	10^9	5×10^8	10^9
α_{gd}	0.30	0.30	0.30	0.30
η_{sat} (m^3 m^{-3})	0.42	0.395	0.451	0.482
ψ_{sat} (m)	-0.299	-0.121	-0.478	-0.405
K_{sat} (m s^{-1})	6.3×10^{-6}	176×10^{-6}	7×10^{-6}	1.3×10^{-6}
b	7.12	4.05	5.39	11.4

over patches of agricultural land in the southwest of France during early summer 1986. They measured the forcing variables required by the model as well as the surface fluxes. A detailed description of these stations and their performance can be found in Goutorbe (1991).

The particular site at Caumont used for the validation was chosen for its reasonable horizontal fetch (as can be seen in Bessemoulin et al. 1987) and for the estimated low error on the net radiation measurements (Goutorbe 1991). Also, this site satisfied the requirement that the two measurement levels used in the computation of the sensible heat flux were not too close to the plant tops, in order to avoid an underestimation of the sensible heat flux due to the presence of the roughness sublayer.

Following data in Mahfouf (1990), a value of 3.2 was attributed to the LAI. Given the plant height of 0.25–0.29 m during the validation period, the roughness length was set to 0.025 m and the displacement height to 0.18 m. The other vegetation parameters were set to values appropriate for crops. The soil parameters are those of a sandy clay loam soil. The initialization of the soil moisture profile was done with neutron-scattering probe data (Goutorbe et al. 1989) that were interpolated to the four soil layers. The moisture data show that the soil close to the surface is very dry, thus inhibiting soil evaporation. However, lower down sufficient soil moisture is available to assure abundant transpiration. The lower boundary condition for soil moisture was set to free drainage.

Figure 2 compares the fluxes calculated by the model with those observed. As the flux plates that measured the soil heat flux were buried a few centimeters under the ground surface, the soil heat flux displayed is the one computed at 0.03-m depth. Furthermore, since the latent heat flux was not directly measured by the SAMER stations but obtained as a residue of the surface energy balance (Goutorbe 1991), the latent heat flux from the SAMER dataset is diminished by the difference between the surface soil heat flux and the soil heat flux at 0.03-m depth (the latter as computed by the model). A scatterplot with the turbulent fluxes is shown in Fig. 3.

Most of the time the model results are within experimental error, estimated to be of the order of 20% (Goutorbe 1991). However, some striking differences between simulation and observation remain. The large negative spikes on the graph of the simulated sensible heat flux are not present in the observational data. This might be caused by advection effects, in spite of the care taken in selecting a site with a good fetch. Another difference between model results and observations is the underestimation of nightly dew production by the model. Other authors (Noilhan and Planton 1989; Mahfouf 1990) have reported the same problem.

b. HAPEX–MOBILHY (Landes) 1 June–21 July 1986

In this validation, the model was forced with data from an automatic weather station operated over a 20-m-high pine forest in the Landes (southwest France), also during the HAPEX–MOBILHY campaign. Simulation results were compared with flux measurements, done with an eddy correlation device, and with soil moisture data. See Gash et al. (1989) for a detailed description of the site and the measurements.

Measurements of the LAI on the trees give a value of $L = 2.3$. However, an understory of bracken, providing a dense cover to the forest floor, was observed to account for 30% of the total transpiration (Granier at al. 1990), leading to the adoption of $L = 6$. (To assess the influence of the uncertainty of this parameter, a sensitivity test was carried out, showing that varying the LAI by ± 1 gives rise to a $\pm 10\%$ change in the latent heat flux.) The roughness length was given a value of 1.6 m and the displacement height set to 14 m. The soil hydraulic parameters correspond to a sandy soil. As there is a clay layer underneath the sand, impeded moisture flow conditions were assumed at the model bottom.

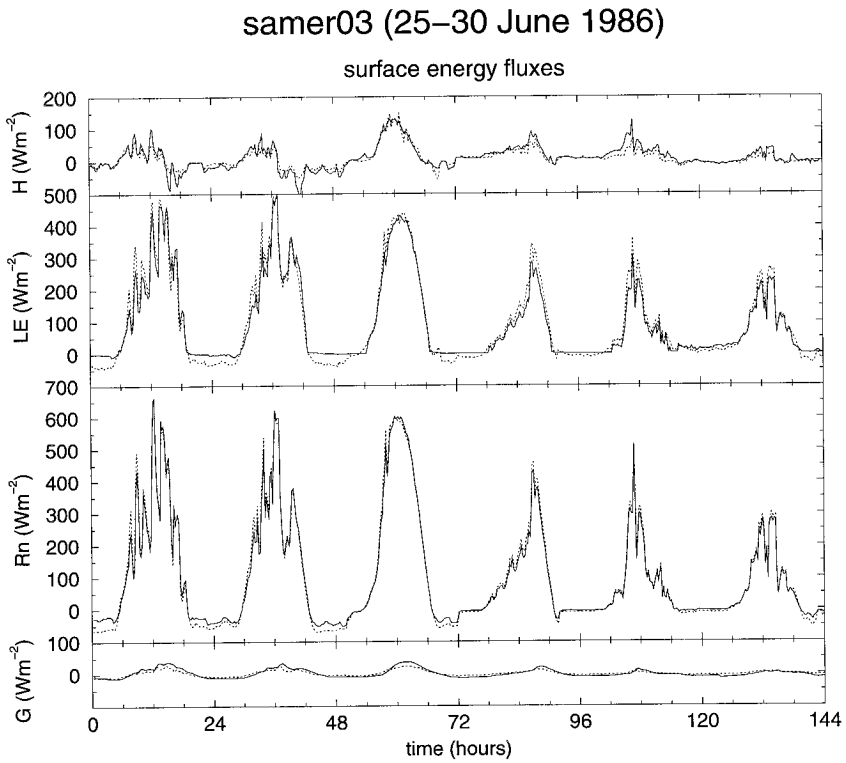

FIG. 2. The simulated (solid line) versus the observed (dotted line) surface energy fluxes for the HAPEX–MOBILHY (Caumont) validation experiment. Shown are the sensible heat flux, the latent heat flux, the net radiation flux, and the soil heat flux.

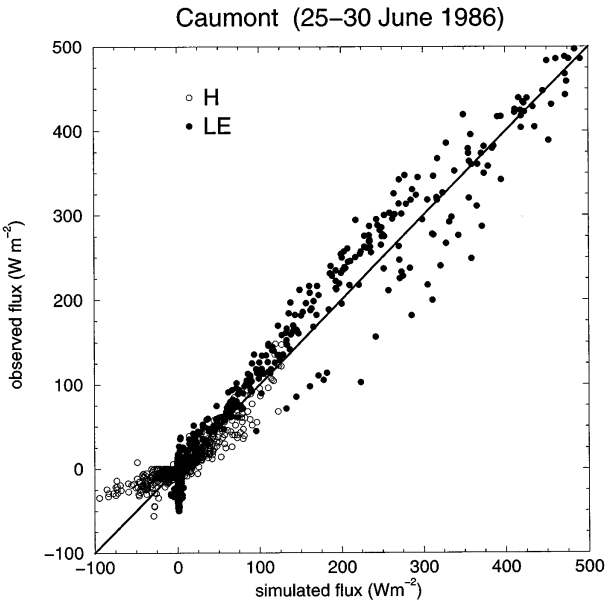

FIG. 3. Scatterplot showing the simulated and the observed sensible (empty circle) and latent (full circle) heat fluxes for the HAPEX–MOBILHY (Caumont) validation simulation.

Since no detailed depth-dependent soil moisture profile was available, the model was initialized uniformly with a mean soil moisture content of 0.22, which is a value given in Gash et al. (1989) for the upper 0.5 m of soil on 1 June.

Figure 4 shows how model-computed soil water content averaged over the upper 0.5 m of soil compares with the measurements. The model follows quite well the measurements during the drying-out period that oc-

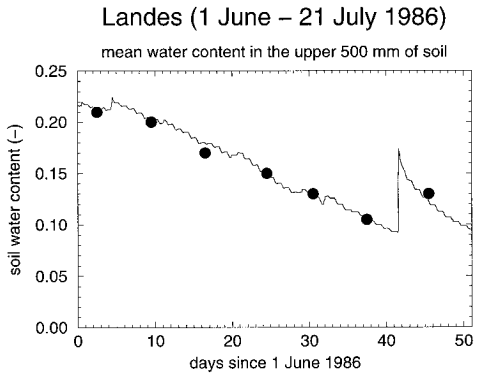

FIG. 4. Average soil moisture content of the upper 0.5 m of soil as simulated by the model (solid line) and as measured (dots) for the HAPEX–MOBILHY (Landes) validation experiment.

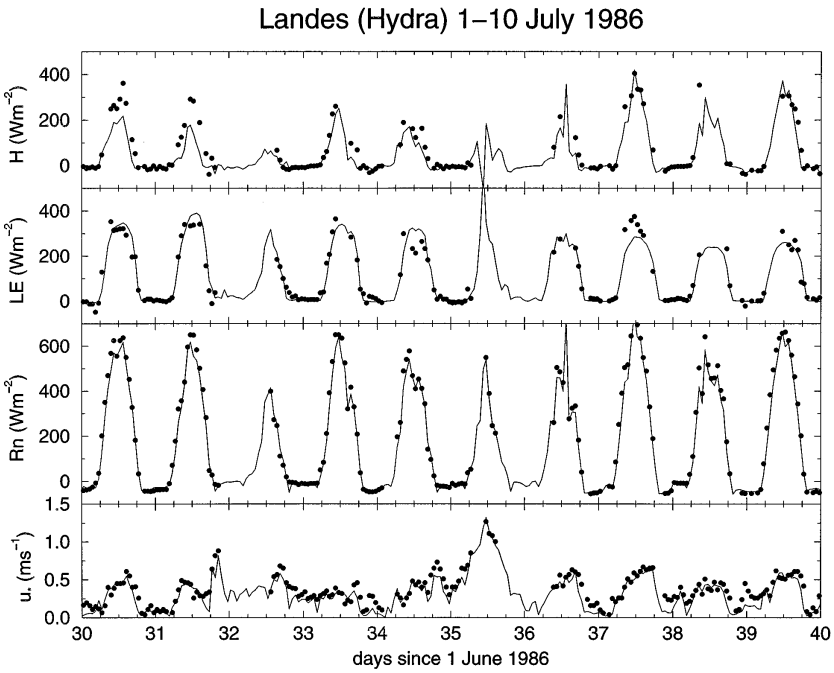

FIG. 5. The simulated (solid line) versus the observed (dots) surface energy fluxes and friction velocity for the HAPEX–MOBILHY (Landes) validation experiment. Shown are the sensible heat flux, the latent heat flux, the net radiation flux, and the friction velocity.

curred from the start up to 42 days later. During this period some minor rainfall was measured that can be seen as small increases in soil water content. The small diurnal fluctuations in the simulated soil moisture curve correspond to transpiration extraction. After 42 days, very high rainfall rates were recorded, up to 32 kg m^{-2} in an hour. It is found that the model handles the subsequent increase in soil moisture quite well.

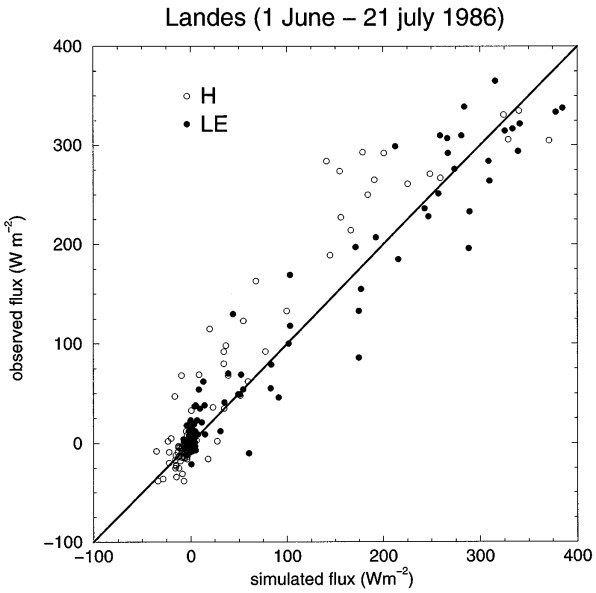

FIG. 6. Scatterplot showing the simulated and the observed sensible (empty circle) and latent (full circle) heat fluxes for the HAPEX–MOBILHY (Landes) validation simulation.

Figure 5 shows the simulated and measured fluxes of sensible and latent heat and net radiation as well as the friction velocity for 1–10 July. Note that the measurements (that are hourly averages) are not equally well distributed in time. The reason, besides the fact that sometimes data are missing (e.g., during rain), is that a selection was performed on the data. Indeed, despite the fact that the energy fluxes close the measured surface energy balance at the daily timescale, such is not always the case at the hourly scale, even when accounting for storage of energy in the ground, the vegetation, and the canopy air. Moore and Fish (1986), for the Amazonian tropical forest, estimated that hourly changes in total heat storage can account for up to ± 80 W m^{-2} of the surface energy budget. Therefore, only those measurements that satisfy $|R_n - H_a - L_vE_a| \leq 80$ W m^{-2} are displayed. Generally, the agreement between the simulated and measured turbulent energy fluxes is satisfactory, although the model seems to overestimate the evaporation flux at the beginning and to underestimate it near the end of the period for which results are shown. During the day, the net radiation is almost systematically slightly underestimated, which may be due to the limited accuracy of the empirical formula used to compute the downward longwave radiation flux. Another explanation would be an overestimation of the canopy temper-

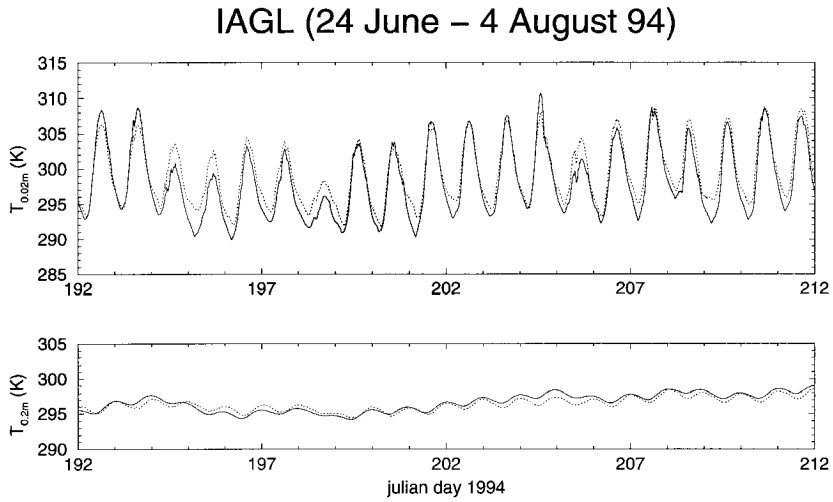

FIG. 7. The simulated (solid line) and observed (dotted line) soil temperatures at the 0.02-m and 0.2-m depths for the IAGL validation experiment.

ature by the model. The simulated friction velocity shows a fair agreement with the data, confirming the validity of the turbulence scheme. Figure 6 shows a scatterplot with the turbulent energy fluxes.

c. IAGL data 24 June–4 August 1994

For this validation experiment, the model was forced with data from the Louvain-la-Neuve meteorological station operated by the IAGL (30 km south of Brussels, Belgium). The surface consists of a loam soil covered by short grass. The variables used in this validation are the soil temperatures at the 0.02- and 0.2-m depths. The instrumental error on these variables is 0.3 K. Note that for certain wind directions this site has fetch problems, due to the presence of tall buildings at a relatively short distance. Observations have shown that the roughness length varies more than an order of magnitude following the wind direction. Therefore, this validation shows what error can be expected on one of the model variables, in this case the soil temperatures, when limited surface parameter information is available, as is mostly the case in mesoscale atmospheric applications.

Visual inspection of the site revealed a fractional vegetation cover between 80% and 90%, so an LAI of 3.5 was chosen. Given a vegetation height of about 0.1 m, values of 0.01 m and 0.07 m were adopted for the roughness length and the displacement height, respectively. In this region the soil is loamy and the hydraulic parameters were chosen accordingly. We assumed free drainage at the model bottom. Since no information about soil moisture was available, the soil was initialized with a uniform profile at half its saturated value, and model results are shown only after the occurrence of some heavy showers. The strong water forcing provided by the latter presumably forces the moisture profile enough for it to become almost independent of the initial state. The soil initial temperature was interpolated from measured data.

Simulated and measured soil temperatures are displayed in Fig. 7. In general, the simulated amplitude and phase of the temperature at the two depths compare well with the data. The discrepancies observed in the absolute values are most likely due to the limited accuracy of the downward longwave flux parameterization and the previously mentioned problem of the wind direction dependence of the roughness length. The root-mean-square errors for the temperatures at the 0.02-m and 0.2-m depths are 1.36 and 0.86 K, respectively. Note that, despite the uncertainties involved, the model reproduces the soil temperature close to the surface with an error of at most 3 K. This is comparable with the error on the surface temperature retrieved from satellite measured radiances (Price 1984), showing that regional scale simulations with the land surface model could be validated with remotely sensed surface temperature data.

d. ARME 1 May–31 August 1985

The last validation experiment shown here was carried out with data gathered over the Amazonian rainforest in Brazil during the ARME campaign (Shuttleworth 1984) and covers 4 months. More than 600 mm of rainfall was recorded during this period.

The LAI was given a value of 6, the roughness length was set to 2 m, and the displacement height to 21 m. The soil hydraulic parameters attributed to the lateritic soil were those of clay. The lower boundary condition for soil moisture is free drainage, as mentioned in Shuttleworth (1988). According to soil tension measurements averaged over the upper 1 m of soil, the model

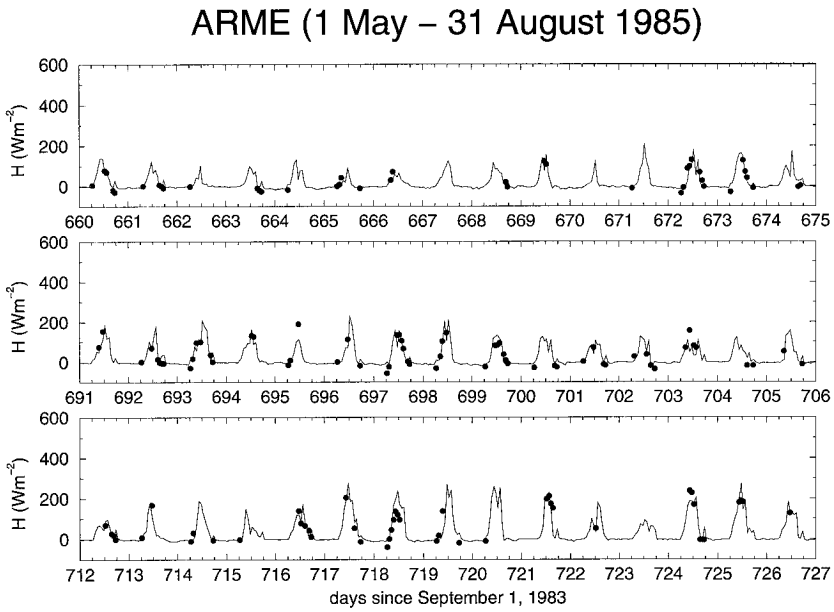

FIG. 8. The simulated (solid line) and observed (dots) sensible heat flux for the ARME validation experiment.

was initialized with a uniform soil moisture content of 0.36.

Figures 8 and 9 compare the simulated and the observed sensible and latent heat fluxes for three 15-day periods. These periods were selected because of their relatively high data coverage. We applied the same procedure as in the HAPEX–MOBILHY (Landes) validation in order to assure energy balance closure of the flux data within 80 W m^{-2}. The overall correspondence with the observations is reasonably good, and most of the time within the 80 W m^{-2} limit of the data. Our main conclusion from this graph is that the model is capable of handling large quantities of water traveling through the soil–plant–atmosphere system and that even after several months simulation there is no significant bias toward an anomalously wet or dry situation.

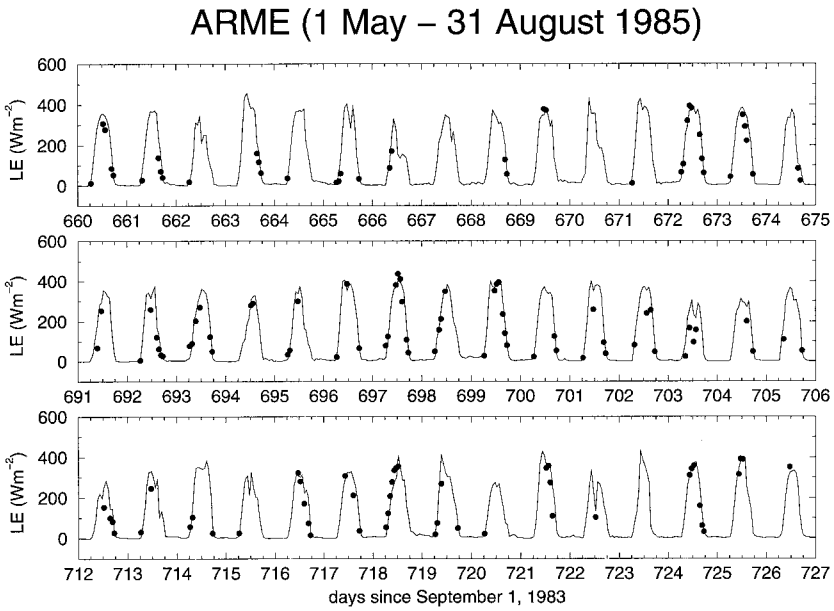

FIG. 9. The simulated (solid line) and observed (dots) latent heat flux for the ARME validation experiment.

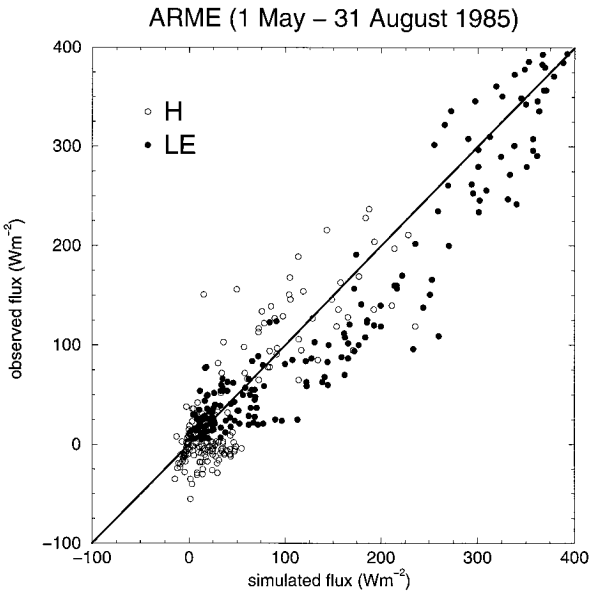

FIG. 10. Scatterplot showing the simulated and the observed sensible (empty circle) and latent (full circle) heat fluxes for the ARME validation simulation.

A scatterplot with the simulated and observed turbulent energy fluxes is shown in Fig. 10.

4. Conclusions

In this paper, a land surface model of intermediate complexity has been described. It combines a simple turbulence transfer scheme with a rather sophisticated transpiration and soil water scheme. The number of parameters to be specified was kept as small as possible while preserving the essential physics of the soil–vegetation–atmosphere exchange processes. The most particular feature of the model is the use of a physically based parameterization of the transpiration process, requiring only one empirical function in the stomatal resistance formulation. It is shown that this parameterization implicitly accounts for stomatal stresses related to visible radiation, soil moisture, saturation deficit, and leaf temperature, and that is consistent with Monteith's (1995) conductance model.

A validation study has shown that the model is reasonably capable of reproducing observed fluxes, despite the fact that no parameter tuning was done and that no explicit saturation deficit and leaf temperature effects on the stomatal resistance were accounted for. The average error on the simulated midday turbulent fluxes is estimated to be of the order of 20%, which is close to instrumental error. The parameters were chosen prior to the simulations, and no tuning was done.

The development and validation of the model presented in this paper forms part of a research project that aims at a better understanding of the influence of the continental land surface, in particular when covered by vegetation, on regional weather and climate. The surface model does not present an excessive computational burden when used in a mesoscale atmospheric model. For instance, when operating the coupled land surface–atmosphere model with time steps of 300 s for the surface scheme and 40 s for the atmosphere model, the former takes about 1% of the total computing time. In the near future, the coupled land surface–atmosphere model will be used in mesoscale modeling studies.

Acknowledgments. We are very grateful to Drs. J.-P. Goutorbe and J. Gash for putting the HAPEX–MOBILHY and ARME data at our disposal and for their helpful comments, and to Jan Dormaels for his help with the IAGL meteorological station data. We also would like to express our gratitude toward Dr. A. Robock, Dr. P. Duynkerke, and M. Lopez-Novella for comments on an early draft of this paper. One of us (KDR) is financed by the Fonds pour la formation à la Recherche dans l'Industrie et l'Agriculture, which is acknowledged.

APPENDIX A

List of Symbols

c_p	specific heat of air at constant pressure (J kg^{-1} K^{-1})
c_w	specific heat of liquid water (J kg^{-1} K^{-1})
d	displacement height (m)
d_i	thickness ith soil layer (m)
D	hydraulic diffusivity (m^2 s^{-1})
drip	leaf drip water flux (kg m^{-2} s^{-1})
E_a	surface vapor flux (kg m^{-2} s^{-1})
$E_{\rm dir}$, $E_{\rm tr}$	direct and transpiration canopy vapor flux (kg m^{-2} s^{-1})
E_g, E_v	ground and canopy vapor flux (kg m^{-2} s^{-1})
g	gravitational acceleration (m s^{-2})
g_v	green leaf fraction
G_g	ground surface heat flux (W m^{-2})
h_g	ground surface relative humidity
H_a	surface sensible heat flux (W m^{-2})
H_g, H_v	ground and canopy sensible heat flux (W m^{-2})
k	von Kármán's constant
K	soil hydraulic conductivity (m s^{-1})
$K_{\rm sat}$	saturated hydraulic conductivity (m s^{-1})
L	leaf area index (LAI) (m^2 m^{-2})
L_e	effective leaf area index (m^2 m^{-2})
L_v	latent heat of vaporization (J kg^{-1})
q_a	specific humidity at reference height (kg kg^{-1})
rain	rainwater flux (kg m^{-2} s^{-1})
r_{am}, r_{ah}	aerodynamic resistance for momentum and heat (s m^{-1})
r_{ag}, r_{av}	ground and canopy aerodynamic resistance for heat (s m^{-1})

r_c	canopy stomatal resistance (s m^{-1})
r_p	plant resistance (s)
r_{si}	soil–root resistance ith soil layer (s)
r_0	unstressed leaf stomatal resistance (s m^{-1})
Ri_b	surface-layer bulk Richardson number
R_{lg}, R_{lv}	longwave energy balance of the ground and the vegetation (W m^{-2})
R_n	net radiative energy balance (W m^{-2})
R_{sg}, R_{sv}	shortwave energy balance of the ground and the vegetation (W m^{-2})
R_w	gas constant for water vapor (J kg^{-1} K^{-1})
S_v	canopy heat storage flux (W m^{-2})
T_a	air temperature at reference level (K)
T_{eff}	effective aerodynamic surface temperature (K)
T_g, T_v	ground surface and canopy temperature (K)
T_i	temperature of ith soil layer (K)
u_a	wind speed at reference level (m s^{-1})
u_*	friction velocity (m s^{-1})
w_l	water equivalent of leaf biomass (kg m^{-2})
w_v	canopy intercepted water content (kg m^{-2})
$w_{v\max}$	canopy maximum water holding capacity (kg m^{-2})
W_g	ground surface water flux (kg m^{-2} s^{-1})
$W_{g\max}$	maximum rain infiltration flux (kg m^{-2} s^{-1})
W_v	plant water flux (kg m^{-2} s^{-1})
W_{vi}	water flux from the ith soil layer (kg m^{-2} s^{-1})
z_a	reference level height (m)
z_s	downward pointing vertical coordinate in the soil (m)
z_{0m}	roughness length for momentum (m)
α_g	soil albedo
α_{gd}	dry soil albedo
δ	wet leaf fraction
ϵ_g	ground surface emissivity
ϵ_l	leaf emissivity
η_i	moisture content of ith soil layer
η_{sat}	saturated soil moisture content
$\varphi_{0.1\mathrm{m}}$	fraction of the roots in the upper 0.1 m of soil
φ_i	fraction of the roots in the ith soil layer
μ	soil thermal conductivity (W m^{-1} K^{-1})
ψ	soil water potential (m)
ψ_c	critical leaf water potential (m)
ψ_g, ψ_v	ground surface and canopy water potential (m)
ψ_i	water potential of the ith soil layer (kg m^{-2} s^{-1})
ψ_{sat}	saturated soil water potential (m)
ρ, τ	leaf reflection and transmission coefficients
ρ_a	air density (kg m^{-3})
ρ_w	liquid water density (kg m^{-3})
$(\rho d)_s$	soil volumetric heat capacity (J m^{-3} K^{-1})
σ_v	fractional vegetation cover
τ_a	surface momentum flux (N m^{-2})

APPENDIX B

The ψ_v-based Stomatal Resistance Formulation

In this appendix, it is shown that the ψ_v-based stomatal resistance formulation implicitly accounts for stresses that are related to soil moisture, atmospheric saturation deficit, and canopy temperature. It is also demonstrated that, in case the vegetation does not experience soil moisture stress, the functional form chosen for $F_{\mathrm{st}}(\psi_v$ in the stomatal resistance formulation is consistent with Monteith's (1995) conductance model. For simplicity it will be assumed that no radiation stress is present and that the soil water potential can be represented by a single value, ψ_s. Furthermore, the aerodynamic resistance and the soil–root resistance will be ignored. Recall that the soil water potential is expressed as a negative height, and that large negative values correspond to a dry soil.

The transpiration water flux E can be written in two different ways, once as a canopy–atmosphere flux and once as a soil–canopy flux:

$$E = \rho_a \frac{\Delta q}{r_c} = \rho_w \frac{\psi_s - \psi_v}{r_p}, \tag{B1}$$

with

$$r_c = r_0 \left(1 - \frac{\psi_v}{\psi_c}\right)^{-1}. \tag{B2}$$

Most symbols are explained in the main text and $\Delta q = q_{\mathrm{sat}}(T_v) - q_a$. By conservation of moisture, assuming that none is stored in the plant, one obtains a system of two equations in ψ_v. Solving this system and substituting the solution into the expression for the stomatal resistance, one obtains

$$r_c = r_0 \left(1 - \rho_a \frac{\Delta q}{r_0} \frac{r_p}{\rho_w \psi_c}\right)\left(1 - \frac{\psi_s}{\psi_c}\right)^{-1}. \tag{B3}$$

This shows that the stomatal resistance is an increasing function of $-\psi_s$, meaning that r_c increases when the soil gets dryer, and of Δq, the latter being itself an increasing function of the atmospheric saturation deficit and the canopy temperature.

Now, consider the case of no soil moisture stress, that is, the soil water potential is nearly zero. The transpiration rate is then given by:

$$E = -\rho_w \frac{\psi_v}{r_p}. \tag{B4}$$

Inverting this relation to obtain ψ_v as a function of E, and inserting the resulting ψ_v value into Eq. (B2), one has:

$$r_c = r_0 \left(1 - \frac{r_p}{\rho_w \psi_c} E\right)^{-1}. \tag{B5}$$

By adopting $E_m = -\rho_w \psi_c / r_p$ the stomatal resistance can then be written as:

$$r_c = r_0 \left(1 - \frac{E}{E_m}\right)^{-1}, \qquad \text{(B6)}$$

which in Monteith's (1995) conductance model written in resistance notation.

REFERENCES

Al Nakshabandi, G., and H. Kohnke, 1965: Thermal conductivity and diffusivity of soils as related to moisture tension and other physical properties. *Agric. Meteor.,* **2,** 271–279.

Alpert, P., and M. Mandel, 1986: Wind variability—An indicator for a mesoclimatic climate change in Israel. *J. Climate Appl. Meteor.,* **25,** 1568–1576.

André, J. C., J. P. Goutorbe, and A. Perrier, 1986: HAPEX-MOBILHY: A hydrological and atmospheric experiment for the study of water budget and evaporation flux at the climatic scale. *Amer. Bull. Meteor. Soc.,* **67,** 138–144.

——, P. Bougeault, J.-F. Mahfouf, P. Mascart, J. Noilhan, and J.-P. Pinty, 1989: Impact of forests on mesoscale meteorology. *Philos. Trans. Roy. Soc. London, Ser. B,* **324,** 407–422.

Ben-Gai, T., A. Bitan, A. Manes, and P. Alpert, 1993: Long-term change in October rainfall patterns in Southern Israel. *Theor. Appl. Climatol.,* **46,** 209–217.

Bessemoulin, P., G. Desroziers, M. Payen, and C. Tarrieu, 1987: Atlas des données SAMER. Internal Rep., CNRM, 256 pp. [Available from Meteo-France, CNRM/GMEI, 42 Av. G. Coriolis, F-31057 Toulouse Cedex, France.]

Bornstein, R., P. Thunis, P. Grossi, and G. Schayes, 1996: Topographic vorticity-mode mesoscale-B (TVM) model: Part II: Evaluation. *J. Appl. Meteor.,* **35,** 1824–1834.

Brutsaert, W. H., 1982: *Evaporation into the Atmosphere.* D. Reidel, 299 pp.

Camillo, P. J., 1991: Using one- or two-layer models for evaporation estimation with remotely sensed data. *Land Surface Evaporation, Measurements and Parameterization,* T. J. Schmugge and J.-C. André, Eds., Springer-Verlag, 183–197.

Charney, J. G., 1975: Dynamics of desert and drought in the Sahel. *Quart. J. Roy Meteor. Soc.,* **101,** 193–202.

Clapp, R. B., and G. M. Hornberger, 1978: Empirical equations for some soil hydraulic properties. *Water Resour. Res.,* **14,** 601–604.

Cowan, I. R., 1965: Transport of water in the soil-plant-atmosphere system. *J. Appl. Ecol.,* **2,** 221–239.

Deardorff, J. W., 1978: Efficient prediction of ground surface temperature and moisture with inclusion of a layer of vegetation. *J. Geophys. Res.,* **83,** 1889–1903.

Denmead, O. T., and E. F. Bradley, 1985: Flux-gradient relationships in a forest canopy. *The Forest–Atmosphere Interaction.* B. A. Hutchinson and B. B. Hicks, Eds., D. Reidel, 443–480.

De Ridder, K., 1997: Radiative transfer in the IAGL land surface model. *J. Appl. Meteor.,* **36,** 12–21.

——, and G. Schayes, 1994: A land surface transfer scheme for use within a mesoscale atmospheric model. *Vegetation, Modelling and Climatic Change Effects,* F. Veroustraete and R. Ceulemans, Eds., Academic Publishing, 187–203.

Dickinson, R. E., 1983: Land surface processes and climate—Surface albedos and energy balance. *Advances in Geophysics,* Vol. 25, Academic Press, 305–353.

Dorman, J. L., and P. J. Sellers, 1989: A global climatology of albedo, roughness length, and stomatal resistance for atmospheric general circulation models as represented by the Simple Biosphere model (SiB). *J. Appl. Meteor.,* **28,** 833–855.

Federer, C. A., 1979: A soil–plant–atmosphere model for transpiration and availability of soil water. *Water Resour. Res.,* **15,** 555–562.

Gallée, H., 1995: Simulation of the mesocyclonic activity in the Ross Sea, Antarctica. *Mon. Wea. Rev.,* **123,** 2051–2069.

——, and G. Schayes, 1994: Development of a three-dimensional meso-gamma primitive equations model, katabatic winds simulation in the area of Terra Nova Bay, Antarctica. *Mon. Wea. Rev.,* **122,** 671–685.

Garrat, J. R., 1992: *The Atmospheric Boundary Layer.* University Press, 316 pp.

Gash, J. H. C., W. J. Shuttleworth, C. R. Lloyd, J.-C. André, J.-P. Goutorbe, and J. Gelpe, 1989: Micrometeorological measurements in Les Landes forest during HAPEX–MOBILHY. *Agric. For. Meteor.,* **46,** 131–147.

Goutorbe, J.-P., 1991: A critical assessment of the SAMER network accuracy. *Land Surface Evaporation, Measurements and Parameterization,* T. J. Schmugge and J.-C. André, Eds., Springer-Verlag, 171–182.

——, J. Noilhan, C. Valancogne, and R. H. Cuenca, 1989: Soil moisture variations during HAPEX-MOBILHY. *Ann. Geophys.,* **7,** 415–426.

Granier, A., V. Bobay, J. H. C. Gash, J. Gelpe, B. Saugier, and W. J. Shuttleworth, 1990: Vapour flux density and transpiration rate comparisons in a stand of Maritime pine (*Pinus pinaster* Ait.) in Les Landes forest. *Agric. For. Meteor.,* **51,** 309–319.

Groot, A., and K. M. King, 1993: Modeling the physical environment of tree seedlings on forest clearcuts. *Agric. For. Meteor.,* **64,** 161–185.

Hillel, D., 1971: *Soil and Water. Physical Principles and Processes.* Academic Press.

Kandel, R., and M.-F. Courel, 1984: Le Sahel est-il responsable de sa sécheresse? *La Recherche,* **158,** 1152–1154.

Lare, A. R., and S. E. Nicholson, 1994: Contrasting conditions of surface water balance in wet years and dry years as a possible land surface–atmosphere feedback mechanism in the West African Sahel. *J. Climate,* **7,** 653–668.

Louis, J. F., 1979: A parametric model of vertical eddy fluxes in the atmosphere. *Bound.-Layer Meteor.,* **17,** 187–202.

Mahfouf, J.-F., 1990: A numerical simulation of the surface water budget during HAPEX-MOBILHY. *Bound.-Layer Meteor.,* **53,** 201–222.

McCumber, M. C., and R. A. Pielke, 1981: Simulation of the effects of surface fluxes of heat and moisture in a mesoscale numerical model. Part I: Soil layer. *J. Geophys. Res.,* **86,** 9929–9983.

Monteith, J. L., 1995: Accomodation between transpiring vegetation and the convective boundary layer. *J. Hydrol.,* **166,** 251–263.

——, and M. H. Unsworth, 1990: *Principles of Environmental Physics.* Edward Arnold, 291 pp.

Moore, C. J., and G. Fish, 1986: Estimating heat storage in Amazonian tropical forest. *Agric. For. Meteor.,* **38,** 147–168.

Nicholson, S. E., 1988: Land surface atmosphere interaction: Physical processes and surface changes and their impact. *Prog. Phys. Geogr.,* **12,** 36–65.

Noilhan, J., and S. Planton, 1989: A simple parameterization of land surface processes for meteorological models. *Mon. Wea. Rev.,* **117,** 536–549.

Otterman, J., A. Manes, S. Rubin, P. Alpert, and D. O'C. Starr, 1990: An increase of early rains in Southern Israel following land use change? *Bound.-Layer Meteor.,* **53,** 333–351.

Pielke, R. A., 1984: *Mesoscale Meteorological Modeling.* Academic Press, 612 pp.

Price, J. C., 1984: Land surface temperature measurements from the split window channels of the *NOAA 7* advanced very high resolution radiometer. *J. Geophys. Res.,* **89,** 7231–7237.

Ralston, A., and P. Rabinowitz, 1978: *A First Course in Numerical Analysis.* McGraw-Hill, 556 pp.

Savijarvi, H., 1992: On surface temperature and moisture prediction in atmospheric models. *Beitr. Phys. Atmos.,* **65,** 281–292.

Schayes, G., P. Thunis, and R. Bornstein, 1996: Topographic vorticity-

mode mesoscale-B (TVM) model. Part I: Formulation. *J. Appl. Meteor.,* **35,** 1815–1823.

Segal, M., and R. W. Aritt, 1992: Nonclassical mesoscale circulations caused by surface sensible heat-flux gradients. *Bull. Amer. Meteor. Soc.,* **73,** 1593–1604.

Sellers, P. J., and J. L. Dorman, 1987: Testing the simple biosphere model (SiB) using point micrometeorological and biophysical data. *J. Climate Appl. Meteor.,* **26,** 622–651.

——, Y. Mintz, Y. C. Sud, and A. Dalcher, 1986: A simple biosphere model (SiB) for use within general circulation models. *J. Atmos. Sci.,* **43,** 505–531.

Shawcroft, R. W., and Lemon, E. R., 1973: Estimation of internal crop water status from meteorological and plant parameters. *Plant Response to Climatic Factors*, R. O. Slatyer, Ed., UNESCO, 449–559.

Shuttleworth, W. J., 1988: Evaporation from Amazonian rainforest. *Proc. Roy. Soc. London, Ser. B,* **233,** 321–346.

——, and coauthors, 1984: Eddy correlation measurements of energy partition for Amazonian forest. *Quart. J. Roy. Meteor. Soc.,* **110,** 1143–1162.

Stull, R. B., 1991: Static stability—An update. *Bull. Amer. Meteor. Soc.,* **72,** 1521–1529.

Viterbo, P., and A. C. M. Beljaars, 1995: An improved land surface parameterization scheme in the ECMWF model and its validation. *J. Climate,* **8,** 2716–2748.

Walker, J., and P. R. Rowntree, 1977: The effect of soil moisture on circulation and rainfall in a tropical model. *Quart. J. Roy. Meteor. Soc.,* **103,** 29–46.

Wetzel, P. J., and J.-T. Chang, 1988: Evapotranspiration from nonuniform surfaces: A first approach for short-term numerical weather prediction. *Mon. Wea. Rev.,* **116,** 600–621.

Wilson, M. F., and A. Henderson-Sellers, 1985: A global archive of land cover and soils data for use in general circulation climate models. *J. Climatol.,* **5,** 119–143.

Yan, H., and R. A. Anthes, 1988: The effect of variations in surface moisture on mesoscale circulations. *Mon. Wea. Rev.,* **116,** 192–208.